Korean J. Chem. Eng., 33(1), 238-247 (2016)
DOI: 10.1007/s11814-015-0113-z

pISSN: 0256-1115
eISSN: 1975-7220

Application of novel nanobiocomposites for removal of nickel(II) from aqueous environments: Equilibrium, kinetics, thermodynamics and *ex-situ* studies

Lina Rose Varghese, Devlina Das, and Nilanjana Das†

School of Bio Sciences and Technology, Environmental Biotechnology Division, VIT University,
Vellore-632 014, Tamil Nadu, India
(*Received 20 March 2015 • accepted 26 May 2015*)

Abstract−The current study presents a novel approach for the removal of Ni(II) from aqueous environments using plant gum-based (PG) and clay-based (CL) nanobiocomposite (NBC) composed of ZnO nanoparticles and chitosan. Parameters like pH, contact time, temperature, initial metal concentration and adsorbent dosage were optimized. Under optimized conditions, maximum removal of Ni(II) was noted as 90.1% and 95.5% in the case of PG-NBC and CL-NBC, respectively. Equilibrium studies suggested a homogeneous mode of adsorption. Good linearity was observed for the pseudo-first order kinetic model, suggesting a physical mode of adsorption. Thermodynamic studies showed an endothermic and spontaneous nature of adsorption. The mechanism was further elucidated using SEM, EDX, AFM and FT-IR analysis. *Ex-situ* studies showed a maximum Ni(II) removal of 87.34% from electroplating wastewater using CL-NBC in column mode. Regeneration studies suggested that CL-NBC could be consistently reused up to 4 cycles.

Keywords: Adsorption, Nanobiocomposite (NBC), Nickel(II), Wastewater

INTRODUCTION

Nickel(II) is a toxic heavy metal present in wastewater derived from various industries such as nickel-cadmium batteries, electroplating, plastic manufacturing, mining and metallurgical processes, plastics manufacturing, fertilizers, porcelain enamelling, and steam electric power plants [1]. Ni(II) is reported to be a potent carcinogen, leading to cancer in the lungs, nose, stomach and bones [2]. Acute nickel poisoning causes headache, dizziness, nausea, vomiting, chest pain and dry cough, shortness of breath, rapid respiration, cyanosis and extreme weakness [3]. The nickel-containing effluents released from the above mentioned industries are highly toxic to both fauna and flora, and therefore require treatment prior to discharge [4]. Over the past few decades, the main technologies used for the treatment of nickel bearing wastewaters include precipitation, ion-exchange, reverse osmosis, electrodialysis and ultrafiltration [5]. All these methods are associated with several disadvantages, such as high operational cost, high consumption of energy, low selectivity and generation of secondary metabolites [6]. Thus, there is a need to search for a cost effective and eco-friendly alternative technique for the removal of Ni(II) from aqueous environments.

Adsorption has been widely applied as an economical and efficient method for the removal of heavy metals from aqueous environments [7]. Recently, applications of nanobiocomposites have received increasing attention as potential adsorbents towards reducing environmental pollution, which incorporates the advantages of both biopolymers and nanoparticles [8]. Biopolymer-based composites have been reported as promising adsorbents for the treatment of wastewater since they show improved properties such as biodegradability and non-toxicity. Various biopolymers and nanoparticles, or a combination of both, have been reported for the removal of pollutants like dyes [9], pesticides [10], heavy metals [11, 12] and anions [13] from aqueous environments. Clay-based nanocomposites have become the materials of interest due to their nanosized structural and functional properties. Clays are known for their high adsorption potential and cation exchange capacities [14]. Reports are available on the use of various types of clays for the removal of Ni(II) [15,16]. However, no report is available on the use of clays as a composite with chitosan and zinc oxide nanoparticles. Gum acacia, a well-known polysaccharide obtained from the stems and branches of Acacia Senegal tree is highly biocompatible, cost effective and ecofriendly [17]. The role of plant-gum based nanobiocomposite has not been exploited as an important adsorbent for the removal of Ni(II) from aqueous environments. To the best of our knowledge, no report is available on the application of nanobiocomposites for the removal of Ni(II) ions from aqueous solutions.

Therefore, the main objective of our study was to compare the potential of plant-gum based nanobiocomposite (PG-NBC) and clay-based nanobiocomposite (CL-NBC) towards the removal of the Ni(II) from aqueous solutions. The adsorption of Ni(II) ions onto PG-NBC and CL-NBC was studied in batch experiments. Adsorption isotherms and kinetics models were studied to describe the experimental data. The mechanism of Ni(II) adsorption on NBCs was elucidated using SEM, AFM, EDX and FT-IR analysis. In addition, *ex-situ* studies were also performed to remove Ni(II) from electroplating wastewater in column mode.

†To whom correspondence should be addressed.
E-mail: nilanjana00@lycos.com

EXPERIMENTAL

1. Materials

All chemicals used in the present study including $Zn(NO_3)\cdot 6H_2O$, chitosan, gum acacia, montmorillonite (clay), $Ni(NO_3)_2\cdot 6H_2O$, NaOH and ethanol were of analytical grade and purchased from Sigma Aldrich, India.

2. Preparation of Nanobiocomposite (NBC) Beads

PG-NBC beads were composed of chitosan, plant gum (gum acacia) and ZnO NPs whereas CL-NBC beads composed of chitosan, montmorillonite and ZnO NPs were prepared following a previously described procedure [18] with minor modifications. Zinc oxide nanoparticles (ZnO NP) were synthesized in the plant gum and clay mixture following a previously described method [19] with modifications. Composite beads were formed with chitosan in 8% NaOH solution after which they were thoroughly washed with de-ionized water and dried in a hot air oven at 60 °C overnight.

3. Batch Adsorption Studies

The effect of operating parameters, namely pH (2.0-12.0), contact time (2-36 h), temperature (20-50 °C), initial Ni(II) concentration (100-1,200 mg/L) and adsorbent dosage (1-6 g/L) on the removal of Ni(II), was investigated. At the end of pre-determined time intervals, the samples were centrifuged at 8,000 rpm for 5 min. Residual concentration of Ni(II) present in the supernatant was analyzed using anatomic adsorption spectrophotometer (AAS). The adsorption capacity (q_e) and the removal percentage (R%) of Ni(II) were calculated according to the following equations:

$$q_e = \frac{C_0 - C_e}{M} \times V \quad (1)$$

$$R(\%) = \frac{C_0 - C_e}{C_0} \times 100 \quad (2)$$

where q_e (mg/g) is the amount of metal ion adsorbed on the adsorbent, C_0 and C_e are the initial and equilibrium concentration of metal ions in solution (mg/L), V is the volume (L) of metal ion solution used and M is the weight (g) of the adsorbent used.

4. Equilibrium, Kinetic and Thermodynamic Studies

The equilibrium data were analyzed by using two-parameter isotherms: Langmuir [20], Freundlich [21] and Dubinin-Radush-

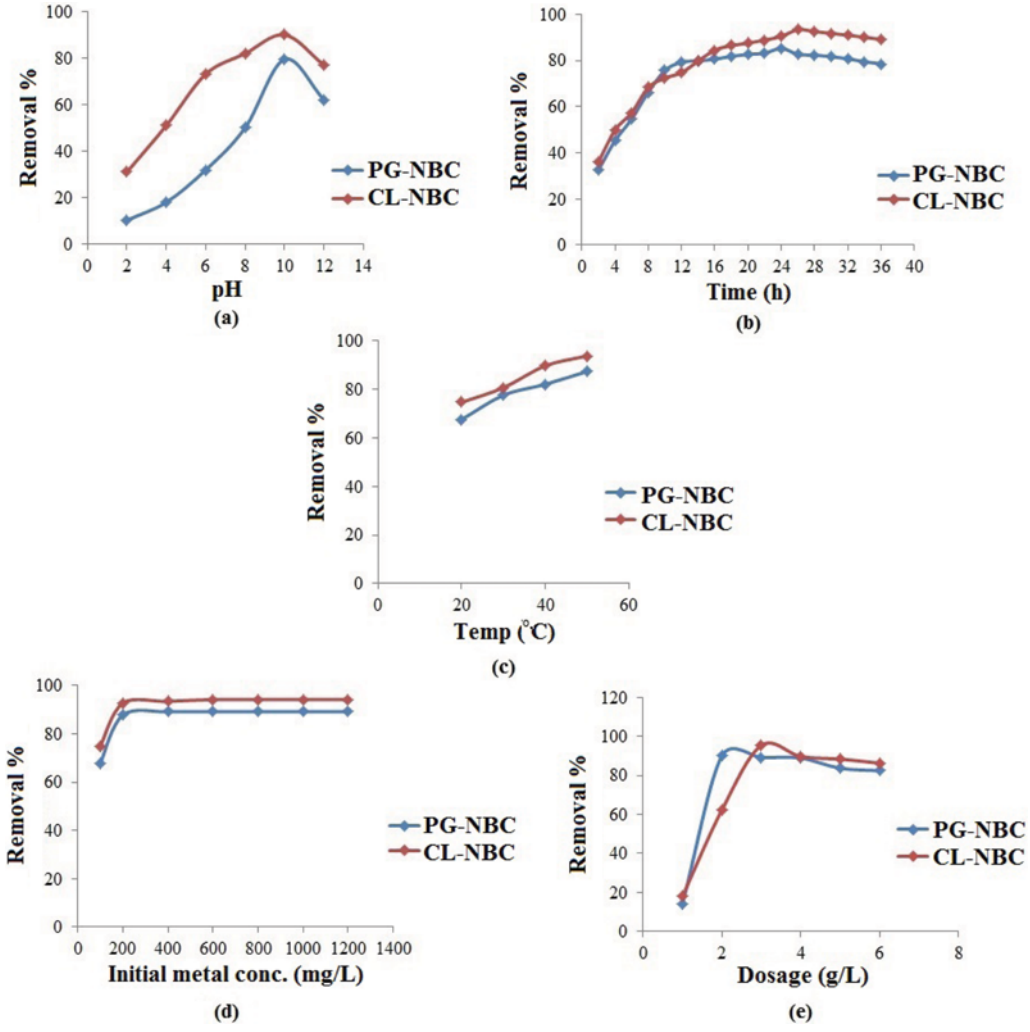

Fig. 1. Effect of (a) pH, (b) contact time, (c) temperature, (d) initial Ni(II) concentration, (e) adsorbent dosage on Ni(II) removal (%) by PG-NBC and CL-NBC.

kevich (D-R) [22]. Kinetic experiments were conducted under optimized conditions and samples were withdrawn at regular intervals for analysis. Pseudo-first order [23] and pseudo-second order [24] models have been used for modelling the kinetic data for adsorption of Ni(II) on nanobiocomposites (NBC). The nature of Ni(II) adsorption was determined by intra-particle diffusion and Boyd Plot [25]. The Gibbs free energy, enthalpy and entropy, (ΔG, ΔH, ΔS) are important thermodynamic parameters with respect to the heat requirements and randomness of the process. The values were obtained from the experiments carried out at different temperatures using the standard equations [26].

5. Instrumental Analysis

The surface morphology of PG-NBC and CL-NBC before and after biosorption of Ni(II) ions was analyzed using scanning electron microscopy (SEM) (Stereo Scan LEO, Model-400). AFM analysis was done using an atomic force microscope (AFM) (Nanosurf-easyscan 2, Netherlands). Fourier transformed infrared spectra were recorded on an Avatar 330 model (Thermo Nicolet Co., USA) FT-IR spectrometer. Each experiment was repeated at least three times. EDAX analyses were conducted using Noran System Six model Energy Dispersive X-Ray Microanalysis System (Thermo Electron Corporation, Japan) attached to SEM. Accelerating voltage was kept constant at 15 kV, to facilitate the emission of secondary X-rays.

6. Effect of Co-ions

The adsorption of Ni(II) was studied in the presence of co-ions: Cu(II) and Cr(VI) in a 2-metal (binary) system and 3-metal (ternary) system. The uptake values of Ni(II) in the presence of co-ions using PG-NBC and CL-NBC were calculated and the experiments were repeated in duplicate. The interaction effects were studied using extended Langmuir and Sheindorf Rebhun Shentuck (SRS) models following the standard equations [27].

7. *Ex-situ* Studies

For *ex-situ* studies, the effluent was collected from an electroplating industry located on the outskirts of Chennai, Tamil Nadu, India. The concentration of Ni(II) in the effluent was analyzed using AAS and the pH was adjusted to 6.0. Experiments were conducted in a glass column (15.0 cm in length) having an internal diameter 3.0 cm which was packed with CL-NBC. The column efficiency was studied at various bed depths (4, 8 and 12 cm), flow rates (1, 3 and 5 ml/min) and dilutions (0%, 25% and 50%). The area under the breakthrough curves was measured to calculate the total metal adsorbed. The total metal sent to the column and the metal removal percentage were calculated by using the standard formula [28].

8. Regeneration Studies

Regeneration experiments were performed using 0.1 M HNO_3 as desorbing agent. After every cycle of adsorption/desorption, the column was washed with de-ionized water until a pH of 7.0 was attained. The experiments were performed using CL-NBC till the efficiency of the column showed a drastic decrease.

RESULTS AND DISCUSSION

1. Effect of Parameters

Maximum removal of Ni(II) ions was noted at pH 10.0 for both PG-NBC and CL-NBC as shown in Fig. 1(a). This could be attributed to the fact that at pH values less than 9.0, nickel is present in the form of Ni^{2+} which results in low adsorption due to the competition between H^+/Na^+ on the surface sites of the biosorbent [29]. The effect of contact time on the removal of Ni(II) was studied, and maximum removal was noted at the end of 24 h for PG-NBC and 26 h for CL-NBC (Fig. 1(b)). The removal of Ni(II) was quite rapid at the beginning due to the abundant availability of active sites on the NBCs, and later became less efficient, which could be due to repulsion between metal ions present in the solution and metal ions adsorbed on the surface of NBC [30]. The effect of temperature on the removal of Ni(II), presented in Fig. 1(c), was found to be at a maximum at 50 °C for both PG-NBC and CL-NBC. The increase in temperature caused a swelling effect within the surface of the NBC and enabled metal cations to penetrate further [31]. Fig. 1(d) shows the effect of initial metal concentration on the removal of Ni(II) ions. An increase in the removal was noted with the increase in initial metal concentration up to 400 mg/L for PG-NBC and 600 mg/L for CL-NBC, beyond which no improvement was noted due to the saturation of the sites on the NBC as the concentration of the metal increased [32]. The dependence of Ni(II) sorption on dosages of PG-NBC and CL-NBC was studied by varying the NBC dosage from 1.0 g to 6.0 g while keeping other parameters constant. Fig. 1(e) showed that the removal of Ni(II) increased with an increase in NBC dosage which could be explained by the

Table 1. Equilibrium isotherm model and kinetic model parameters for Ni(II) adsorption on PG-NBC and CL-NBC

	Parameters	PG-NBC	CL-NBC
Isotherm models	q_m (mg/g)	188.67	232.55
Langmuir	K_L (L/mg)	$3.9*10^{-3}$	0.349
	R^2	0.992	0.979
	APE (%)	8.73	4.23
Freundlich	K_F (L/g)	5.341	30.45
	n	1.01	2.65
	R^2	0.757	0.553
	APE (%)	24.49	35.11
Dubinin-Radushkevich	q_m (mg/g)	310.31	212.42
	β (mol^2/J^2)	$1*10^{-4}$	$3*10^{-5}$
	E (kJ/mol)	0.07	0.12
	R^2	0.892	0.980
	APE (%)	76.55	31.13
Kinetic models	q_e (mg/g)	231.7	242.3
Pseudo first order	K_1 (min^{-1})	0.107	0.119
	R^2	0.977	0.954
	APE (%)	1.71	3.96
Pseudo second order	q_e (mg/g)	204.08	344.82
	K_2 (g/mg/min)	$8.13*10^{-4}$	$1.3*10^{-4}$
	R^2	0.950	0.760
	APE (%)	8.923	11.50
Intraparticle diffusion	v	30.90	37.95
	c	26.24	0.607
	R^2	0.981	0.957
	APE (%)	2.48	0.95

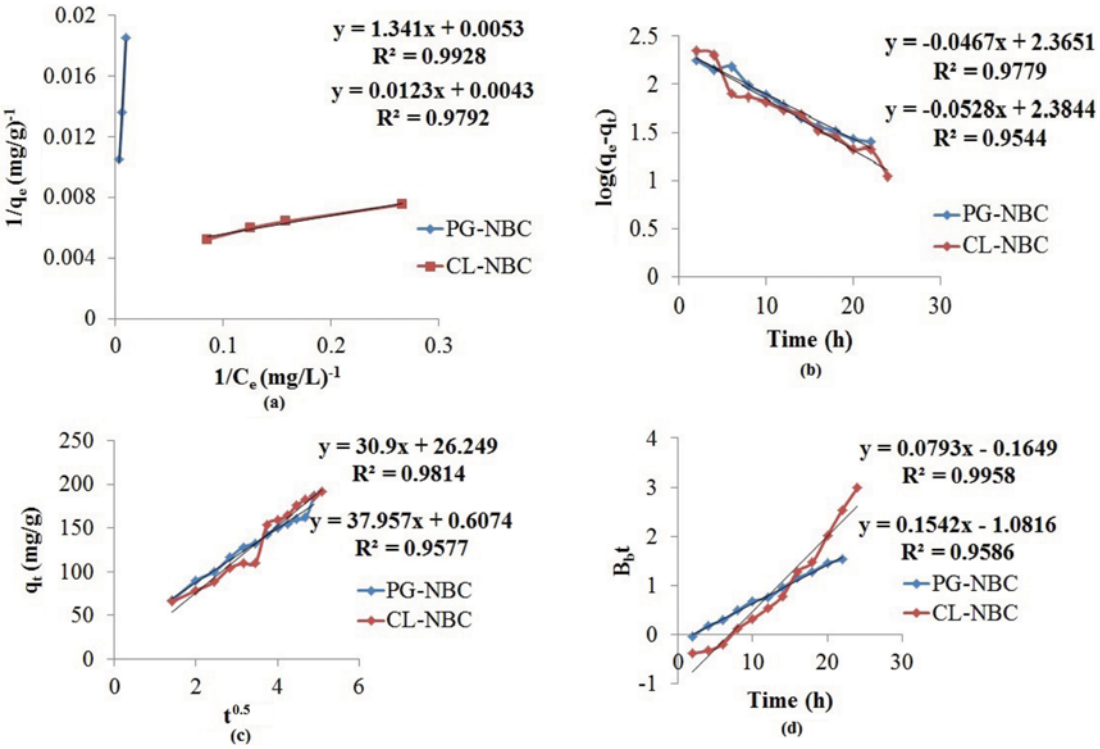

Fig. 2. (a) Langmuir isotherm, (b) pseudo first order kinetics, (c) intraparticle diffusion, (d) boyd plot of Ni(II) adsorption onto PG-NBC and CL-NBC.

availability of more adsorption sites and exchangeable ions for adsorbent-metal ion interaction [33]. Therefore, maximum removal of Ni(II) by PG-NBC and CL-NBC was found to be 90.1% and 95.5%, respectively, under optimized conditions in batch mode.

2. Equilibrium, Kinetic and Thermodynamic Studies

The isotherm and kinetic constants, correlation coefficient values (R^2) and average percentage error values (APE%) were calculated and presented in Table 1. Of the various two-parameter isotherm models tested (Langmuir, Freundlich and Dubinin-Radushkevich (D-R)), the Langmuir model was the most appropriate isotherm to describe the equilibrium data for Ni(II) adsorption for both PG-NBC and CL-NBC (Fig. 2(a)), thereby suggesting a homogeneous and monolayer mode of adsorption owing to their high R^2 values and low APE values. Adsorption of Ni(II) on both the NBCs occurred uniformly on the active sites and no further adsorption took place at a pre-occupied site [34]. The Freundlich model exhibited a poor fit due to low R^2 values and high error values. The data on mean free energy (E) from D-R isotherm model suggested the requirement of a higher amount of energy for the removal of Ni(II) from CL-NBC than PG-NBC, thereby confirming a higher affinity between Ni(II) and CL-NBC. Among the kinetic models, the pseudo-first-order model (Fig. 2(b)) exhibited the best fit owing to their high R^2 values and low APE values, suggesting physisorption as underlying phenomenon for both PG-NBC and CL-NBC. The nature of adsorption was further evaluated by using the intra-particle diffusion model, which exhibited good fit for both the NBCs (Table 1). In the present study, both intra-particle diffusion and film diffusion played a significant role. As shown in Fig. 2(c) and Fig. 2(d), both intra-particle diffusion and Boyd plot showed a

Table 2. Thermodynamics parameters

NBCs	Temperature (K)	ΔG (kJ/mol)	ΔH (kJ/mol)	ΔS (kJ/mol/K)
PG-NBC	283	−1.294	29.27	0.108
	293	−2.374		
	303	−3.454		
	313	−4.534		
	323	−5.614		
CL-NBC	283	2.177	25.10	0.081
	293	1.367		
	303	0.557		
	313	−0.253		
	323	−1.063		

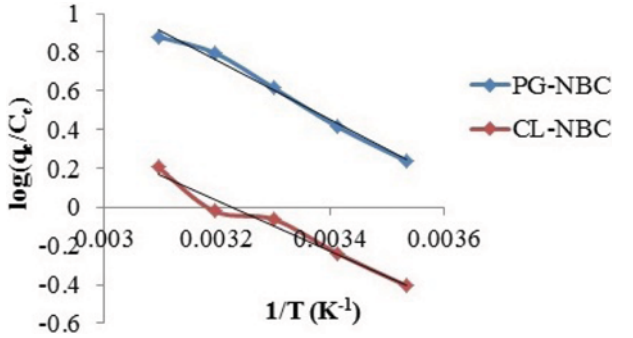

Fig. 3. Thermodynamic studies for adsorption of Ni(II) on PG-NBC and CL-NBC.

good linearity. Moreover, in the case of intra-particle diffusion, the adsorption process was found to occur in five phases for PG-NBC and six phases for CL-NBC. The Boyd curves were found to be quite linear, but they did not pass through the origin, which suggested the involvement of both film diffusion and intra-particle diffusion (Fig. 2(d)).

As shown in Table 2, the process was found to be spontaneous for PG-NBC and CL-NBC, which was indicated by negative ΔG values, and maximum spontaneity was noted at 50 °C for both the NBCs. The values of ΔH and ΔS were calculated from the slope and intercept of the plot of log (q_e/C_e) vs1/T (Fig. 3). The results indicated that the process was endothermic or heat absorbing in nature as indicated by the positive values of ΔH (29.27 kJ/mol for PG-NBC and 25.10 kJ/mol for CL-NBC). An increase in randomness at the solid/solution interface was suggested by the positive value of ΔS.

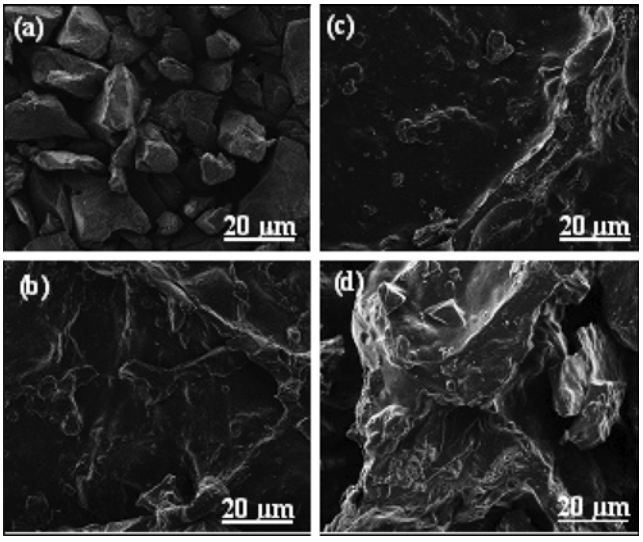

Fig. 4. SEM analysis of (a) PG-NBC (b) CL-NBC before Ni(II) adsorption (c) PG-NBC (d) CL-NBC after Ni(II) adsorption.

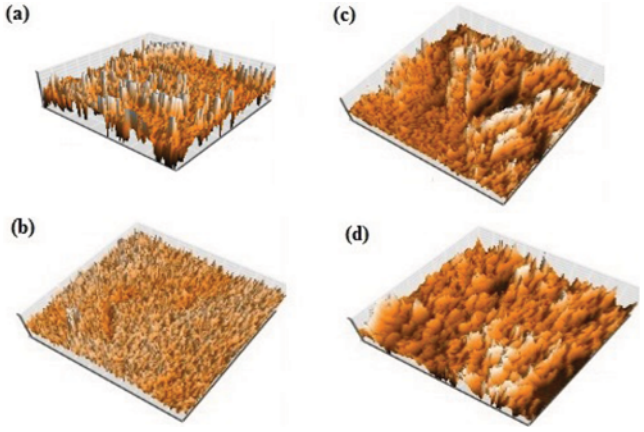

Fig. 5. AFM images of 3D layer of (a) PG-NBC (b) CL-NBC before Ni(II) adsorption (c) PG-NBC (d) CL-NBC after Ni(II) adsorption.

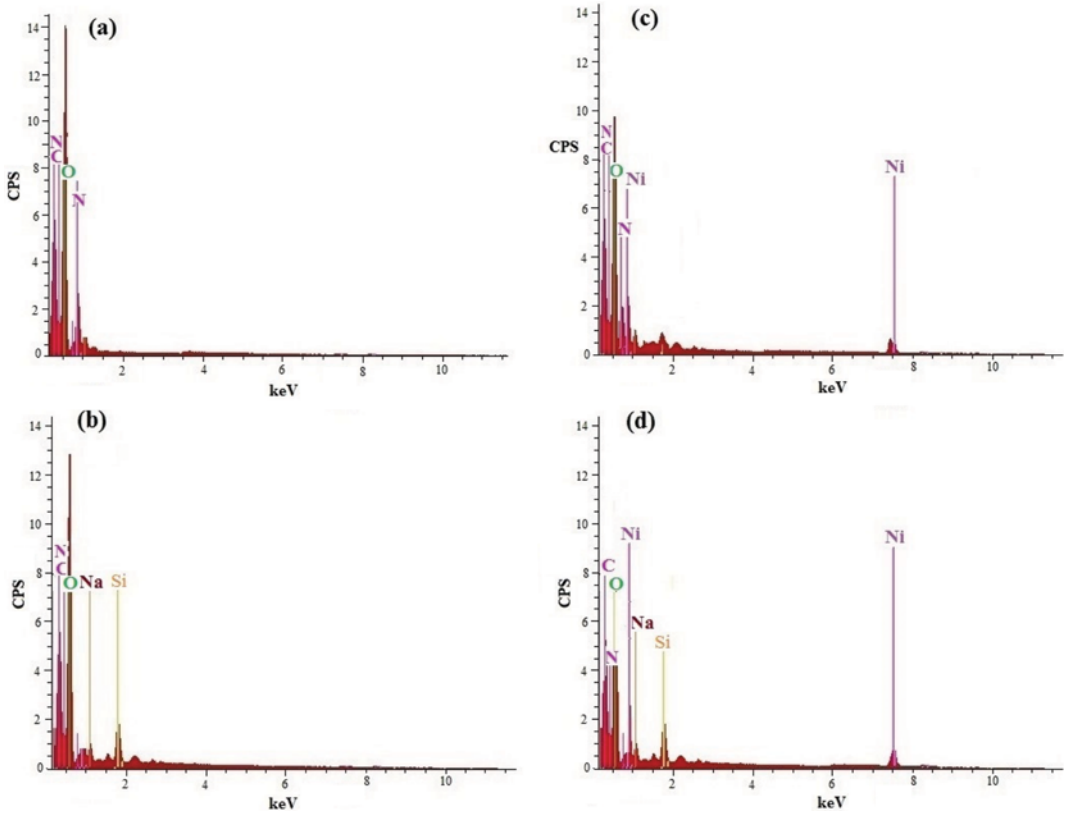

Fig. 6. EDX analysis of (a) PG-NBC (b) CL-NBC before Ni(II) adsorption (c) PG-NBC (d) CL-NBC after Ni(II) adsorption.

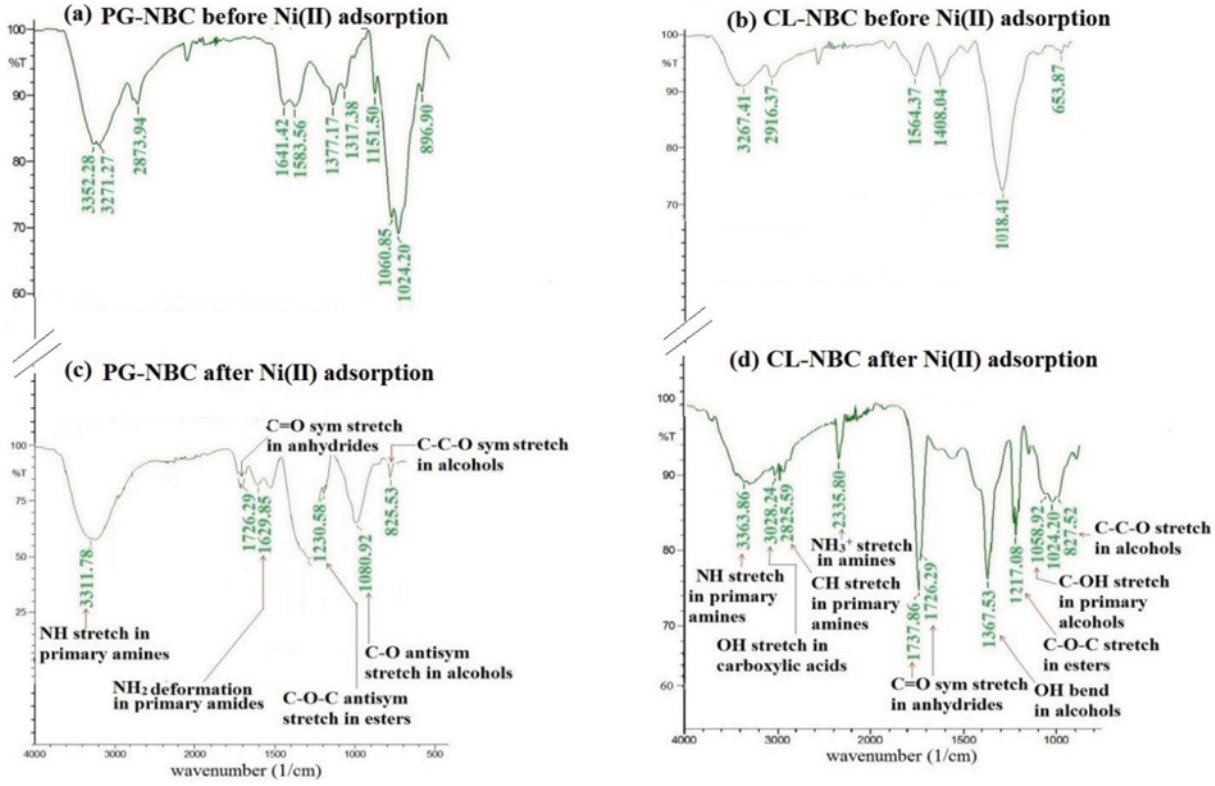

Fig. 7. FTIR analysis of (a) PG-NBC (b) CL-NBC before Ni(II) adsorption (c) PG-NBC (d) CL-NBC after Ni(II) adsorption.

3. Instrumental Analysis

The surface morphologies of PG-NBC and CL-NBC before and after Ni(II) adsorption were studied using scanning electron microscopy. Before biosorption of Ni(II), PG-NBC shows particles of non-uniform shape and size (Fig. 4(a)), whereas after Ni(II) biosorption a completely different morphology was observed (Fig. 4(c)). Similar results were reported for Ni(II) biosorption by gum kondagogu (*Cochlospermumgossypium*) [35]. Fig. 4(b) shows a higher surface area for Ni(II) biosorption onto CL-NBC. A more electron dense part (bright region) was noted for CL-NBC after nickel uptake [36] when compared to PG-NBC, as shown in Fig. 4(d). This was further validated by the atomic force microscopic images of PG-NBC and CL-NBC before and after adsorption of Ni(II) (Fig. 5(a)-(d)). An enhanced surface roughness with uniformity was noted for CL-NBC when compared to PG-NBC, resulting in a higher uptake of Ni(II) ions.

The elemental analysis of PG-NBC and CL-NBC before and after the adsorption of Ni(II) was performed using energy dispersive X-ray (EDX) analysis (Fig. 6(a)-(d)). The EDX spectrum of PG-NBC before Ni(II) adsorption indicated the presence of C, N and O as natural species on the NBC (Fig. 6(a)). The peaks of Si and Na were noted on CL-NBC before Ni(II) adsorption, which confirmed the presence of clay on the NBC (Fig. 6(b)). An intense Ni(II) peak was observed for CL-NBC (Fig. 6(d)) compared to PG-NBC after Ni(II) adsorption (Fig. 6(c)). In the case of CL-NBC, a certain decrease in the peaks of Si and Na after Ni(II) adsorption confirmed their involvement in the adsorption process (Fig. 6(d)). For both the nanobiocomposites, a significant decrease in the N peak was noted, which validated the involvement of N element in the adsorption process. Moreover, a higher decrease in N peak for CL-NBC confirmed the higher uptake potential of CL-NBC compared to PG-NBC.

FT-IR spectra presented in Fig. 7(a)-(d) represent various functional groups present on the surface of PG-NBC and CL-NBC before and after adsorption of Ni(II) ions. A high involvement of primary amines (NH stretch (3,364 cm^{-1}), CH stretch (2,826 cm^{-1}), NH_3^+ stretch (2,336 cm^{-1})) was noted for CL-NBC (Fig. 7(d)) compared to that of PG-NBC after Ni(II) adsorption (Fig. 7(c)). Additional involvement of carboxylic acids (3,028 cm^{-1}), anhydrides (1,738 cm^{-1} and 1,726 cm^{-1}), esters (1,217 cm^{-1}) and alcohols (1,368 cm^{-1}, 1,059 cm^{-1} and 828 cm^{-1}) was noted for CL-NBC. Similar results were reported for Ni(II) adsorption onto *E. coli* biomass [4]. The involvement of amides, anhydrides and esters when using PG-NBC was not found to play an important role in the process of adsorption. The involvement of more functional groups and the changes in the overall transmittance was found to be higher for CL-NBC compared to that of PG-NBC, which validated CL-NBC as a potential adsorbent for the remediation of Ni(II) from wastewater.

4. Effect of Co-ions

Of the two co-ions tested (Cu(II) and Cr(VI)), Cu(II) was found to exhibit a maximum interaction effect on Ni(II) adsorption followed by Cr(VI), owing to their difference in ionic radii. To understand the metal-metal interactions with the adsorbent, an interaction factor (η) was calculated for both binary and ternary systems.

The extended Langmuir and SRS equation parameters for both binary and ternary systems were tabulated and are shown in Table

Table 3. Extended Langmuir and SRS equation parameters for binary and ternary systems

Extended Langmuir				SRS			
	Ni-Cu		**Ni-Cu-Cr**		**Ni-Cu**		**Ni-Cu-Cr**
PG-NBC							
η_1	0.22	η_1	0.37	K_{Fi}	43.72	K_{Fi}	43.72
η_2	3.14	η_2	3.17	η_i	3.62	n_i	3.62
b_1	0.08	η_3	1.07	θ_{ij}	1.5	θ_{ij}	2.4
b_2	0.54	b_1	0.08	APE (%)	5.94	APE (%)	19.40
APE (%)	21.40	b_2	0.54	R^2	1.0	R^2	1.0
R^2	1.0	b_3	0.17				
		APE (%)	26.05				
		R^2	1.0				
CL-NBC							
η_1	0.14	η_1	0.28	K_{Fi}	40.21	K_{Fi}	40.21
η_2	2.09	η_2	2.12	n_i	2.62	n_i	2.62
b_1	0.06	η_3	0.67	θ_{ij}	2.1	θ_{ij}	6.3
b_2	0.41	b_1	0.06	APE (%)	24.79	APE (%)	26.11
APE (%)	39.13	b_2	0.41	R^2	0.992	R^2	0.992
R^2	0.968	b_3	0.43				
		APE (%)	45.95				
		R^2	0.958				

3. Based on the extended Langmuir equation, the interaction factor (η_2) was found to be the highest for PG-NBC (3.14) and CL-NBC (2.09), which signified that copper had the most predominant effect on Ni(II) adsorption. In the case of both CL-NBC and PG-NBC, the interaction factors were found to be higher for the ternary system compared to binary system. Moreover, the interaction factors were found to be lower for CL-NBC, thereby suggesting a lower level of competition between Ni(II) and co-ions compared to that of PG-NBC (Table 3). The results were further validated by the selectivity factors. A maximum factor of 1.35 was noted for CL-NBC, thereby denoting a preferential adsorption of Ni(II) ions as compared to PG- NBC (0.87).

The SRS equation was employed to describe the binary and ternary data to improve the fitness. The competitive coefficient (θ) was found to be higher for the ternary system compared to binary system. Moreover, the competition coefficient was higher in case of CL-NBC as compared to PG-NBC, which validated the adsorption potential of the former over the latter. Results suggested a better distribution of adsorption energies for the metal ions for CL-NBC compared to PG-NBC (Fig. 8).

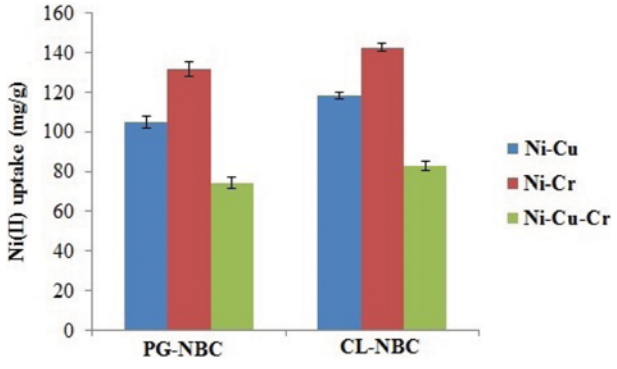

Fig. 8. Effect of co-ions on adsorption of Ni(II) on PG-NBC and CL-NBC.

Based on the error and correlation coefficient values, it could be inferred that the SRS model exhibited a better fit for both CL-NBC and PG-NBC for the binary and ternary systems compared to that of the extended Langmuir model.

5. *Ex-situ* Studies

5-1. Effect of Column Parameters

The removal of Ni(II) using CL-NBC was studied as a function of column parameters: bed height (4 cm, 8 cm and 12 cm), flow rate (1 ml/min, 3 ml/min and 5 ml/min) and effluent dilutions (0%, 25% and 50%). The efficiencies were evaluated in terms of breakthrough time (t_b), exhaustion time (t_e), total amount of pollutant sent to the column (M_{total}), amount of pollutant adsorbed (M_{ad}) and removal (%). Breakthrough curves for the various parameters are presented in Fig. 9(a)-(c). As shown in Table 4, a bed height of 12 cm showed maximum Ni(II) removal of 87.34% at a flow rate of 1 ml/min and 0% dilution. Increase in the bed height led to a considerable increase of both breakthrough time (125-200 min) and exhaustion time (200-250 min), which could be attributed to the fact that a taller bed will have more adsorbent sites to which metal ions could bind [37]. The effect of flow rate on the removal Ni(II) was studied at maximum bed height (12 cm) and 0% dilution. In contrast to the results obtained above, maximum adsorption efficiency was noted at the minimum flow rate (1 ml/min), beyond which a decrease was noted due to the insufficient time allotted for the interaction between pollutant and adsorbent [18]. The effect of various dilutions on Ni(II) adsorption was studied at maximum bed height (12 cm) and minimum flow rate (1 ml/min). The breakthrough time (t_b) and adsorbed metal (M_{ad}) values were found to decrease with an increase in dilution and maximum removal of

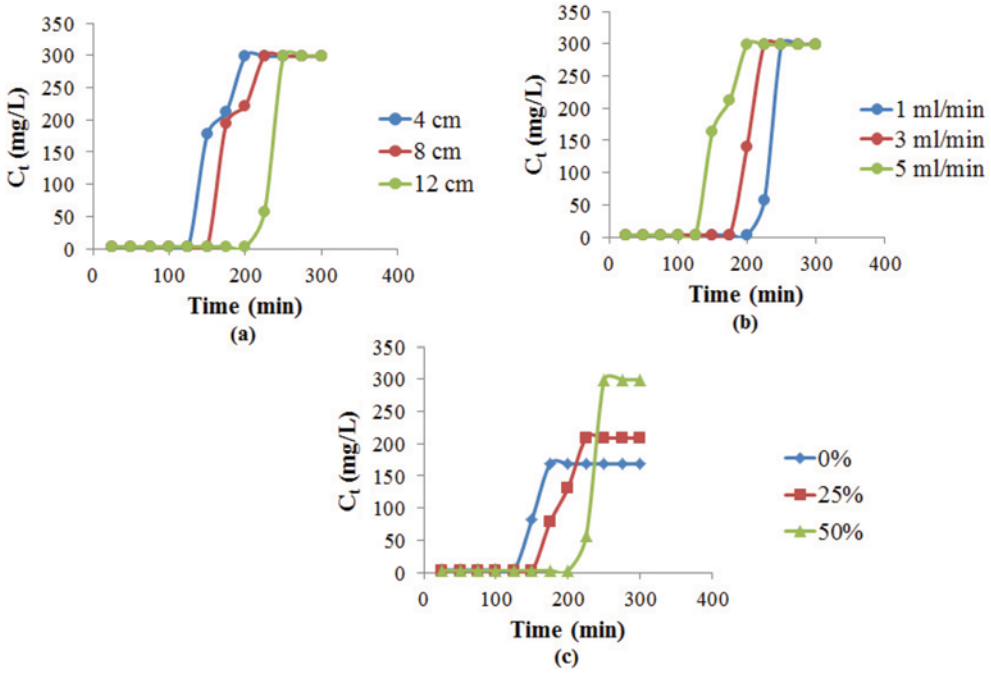

Fig. 9. Breakthrough curves for adsorption of Ni(II) onto CL-NBC.
(a) At different bed heights (flow rate - 1 mL/min, dilution-0%), (b) at different flow rates (bed height - 12 cm, dilution-0%), (c) at different dilutions (bed height 12 cm, flow rate 1 mL/min)

Table 4. Column parameters obtained at different bed heights, flow rates and dilutions for nickel(II) adsorption

	4 cm	**8 cm**	**12 cm**
	Bed height (flow rate-1ml/min; dilution-0%)		
t_b (min)	125	150	200
t_e (min)	200	225	250
M_{total}	60	67.5	75
M_{ad}	42.41	49.18	65.50
Efficiency (%)	70.69	72.86	87.34
	1 ml/min	**3 ml/min**	**5 ml/min**
	Flow rate (bed height-12 cm; dilution-0%)		
t_b (min)	200	175	125
t_e (min)	250	225	200
M_{total}	75	67.5	60
M_{ad}	65.50	55.97	42.74
Efficiency (%)	87.34	83.92	71.23
	0%	**25%**	**50%**
	Dilutions (flow rate-1 ml/min; bed height-12 cm)		
t_b (min)	125	150	200
t_e (min)	175	225	250
M_{total}	52.5	67.5	75.0
M_{ad}	22.96	36.33	65.50
Efficiency (%)	43.74	53.82	87.34

Ni(II) was noted at 0% dilution. In undiluted wastewater (0% dilution), the availability of metal ions is higher, which leads to higher uptake of metal ions when compared to that of diluted wastewater.

5-2. Column Data Modelling

One of the most commonly used adsorption models is the bed depth service time model (BDST), which states the relation between the bed height (cm) and service time (min). The plot of service time vs bed height at various dilutions is presented in Fig. 10(a) maintaining the flow rate of 1 ml/min. The model exhibited an excellent fit owing to an R^2 value greater than 0.98 (Table 5). A decrease in column sorption capacity (N_0) was noticed with an increase in dilution owing to the reduction in the concentration of metal sent through the column. An increase in the rate constant (K_a) was noted with an increase in dilution (up to 50%), which indicated that a considerably shorter bed was required to avoid breakthrough [38].

In the present study, the Thomas model was also used to evaluate column breakthrough data. Based on the plot of $\ln((C_0/C_t)-1)$ vs volume of effluent treated (V_{eff}) shown in Fig. 10(b), the Thomas model parameters were calculated and are presented in Table 5. The model exhibited a good fit owing to an R^2 value of 0.976. The rate constant (K_{TH}), the parameter which identified the rate of transfer of solute from liquid to solid phase, was found to increase with an increase in dilution, which signified a higher sorption rate at a low metal concentration due to the availability of more surface functional groups [38].

Electroplating wastewater analysis was performed using packed bed column under optimum conditions (bed height: 12 cm, flow rate: 1 ml/min and dilution: 50%). A decrease in the overall COD, TDS, chlorides, sulfates and heavy metals was noted as shown in Table 6, which justified the adsorption potential of CL-NBC.

6. Regeneration Studies

The regeneration and reuse of the adsorbent is crucial from an industrial point of view for the reduction of the process cost, the

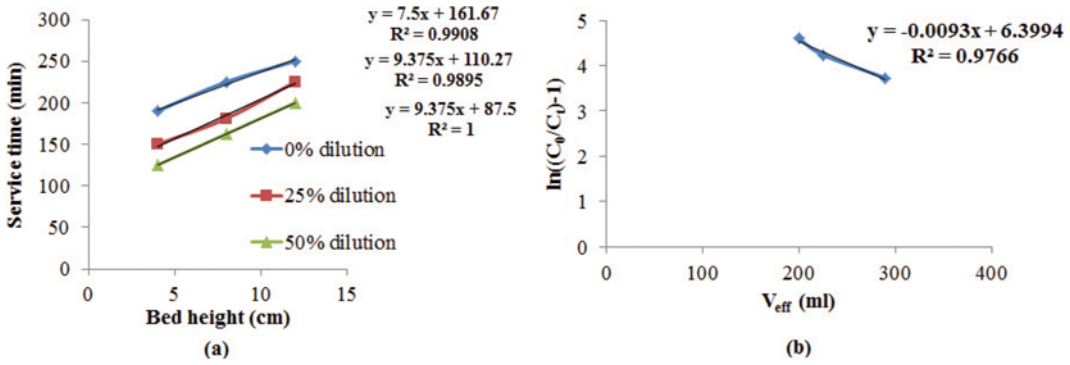

Fig. 10. (a) BDST model (b) Thomas model.

Table 5. Bed depth service time model and Thomas model parameters for adsorption of Ni(II) on CL-NBC at different effluent dilutions

	Effluent dilutions		
	0%	25%	50%
BDST parameters			
Slope	7.500	9.375	9.375
Intercept	175.00	110.27	87.50
N_o (mg/L)	179.77	277.59	396.56
K_a (L/mg/min)	$1.25*10^{-4}$	$1.82*10^{-4}$	$1.75*10^{-3}$
R^2	0.99	0.98	1.00
Thomas parameters			
V_{eff}	200	225	290
C_o	300	210	170
K_{TH} (min^{-1})	$3.10*10^{-5}$	$4.42*10^{-5}$	$5.47*10^{-5}$
Q_o (mg/g)	412.83	289.54	233.96

Table 6. Analysis of electroplating industrial effluent

Parameters	Before treatment with CL-NBC	After treatment with CL-NBC
pH	6.0	6.8
Chemical oxygen demand (mg/L)	728.8±0.20	59.2±0.30
Total dissolved solids (mg/L)	826.6±0.04	45.6±0.10
Sulphate (mg/L)	145.8±0.03	15.1±0.21
Iron Fe^{2+} (mg/L)	100.7±0.01	3.2±0.20
Chlorides (mg/L)	186.5±0.20	47.2±0.30
Copper(II) (mg/L)	186.1±0.03	0.7±0.16
Nickel(II) (mg/L)	300.0±0.25	2.8±0.02
Chromium(VI) (mg/L)	98.2±0.03	3.1±0.34

continuous dependency on the adsorbent and for the possible removal of metal ions. Therefore, attempts were made to regenerate and reuse CL-NBC by using the column mode of operation (Fig. 11). Six cycles of desorption and sorption were performed to study the reusability of the adsorbent. The breakthrough time (t_b), exhaustion time (t_e), removal percentage and desorption percentage for six cycles are summarized in Table 7. A decrease in breakthrough time and exhaustion time was observed as the regeneration cycle progressed. The maximum removal was noted as 87.34%. The CL-

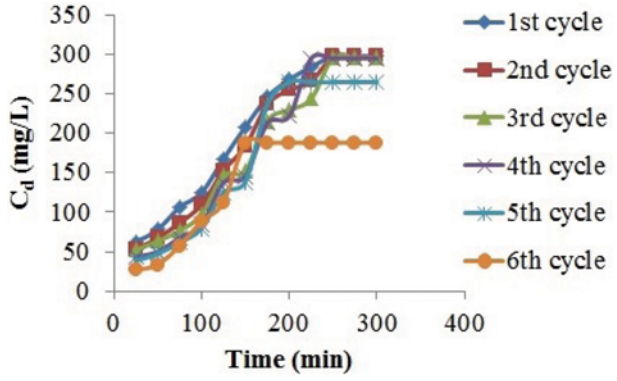

Fig. 11. Reuse of CL-NBC during six regeneration cycle.

Table 7. Adsorption and elution process parameters for different sorption-desorption cycles

Parameters	No. of cycles					
	1	2	3	4	5	6
t_b (min)	200	200	200	175	150	100
t_e (min)	250	250	250	225	200	150
M_{total} (mg)	75.0	75.0	75.0	67.5	60.0	45.0
M_{ad} (mg)	65.50	65.29	64.95	56.99	44.59	21.24
M_d (mg)	42.28	38.94	35.60	27.71	21.48	10.30
Removal (%)	87.34	87.06	86.60	84.42	74.33	47.21
Desprption (%)	56.38	51.92	47.47	41.06	35.80	22.91

NBC could be successfully reused at the end of the fourth cycle. After the fourth cycle, a drastic fall in the removal was noted which could be attributed to the damages on the surface of the CL-NBC due to the continuous contact with the desorbing agent (0.1 M HNO_3).

CONCLUSION

The results of this study demonstrate the application of plant-gum based and clay-based nanobiocomposites (NBC) for the removal of Ni(II) from aqueous environment. Maximum Ni(II) removal of 90.1% for PG-NBC and 95.5% for CL-NBC was noted under optimized condition. Equilibrium sorption data showed an excellent fit to the Langmuir isotherm model, indicating a monolayer mode of Ni(II) adsorption onto the surface of NBCs. The result

of adsorption kinetic studies suggest a physical mode of adsorption via both intra-particle and film diffusion modes. Thermodynamic studies defined the endothermic nature of the process. Maximum removal of 87.34% nickel(II) from electroplating wastewater was noted under optimum conditions (bed height: 12 cm, flow rate: 1 ml/min and dilution 0%) in column mode. Though the removal of nickel (99.9%) is reported using the chemical precipitation method, it may not be accepted due to some drawbacks such as high operational cost, requirement of power and generation of waste products. Therefore, adsorption using NBC may be considered as an excellent and cost effective approach for the removal of Ni(II) from aqueous environments. The regeneration studies indicate that CL-NBC could serve as an efficient and reliable adsorbent for the remediation of Ni(II) ions from wastewater.

ACKNOWLEDGEMENTS

The authors gratefully acknowledge VIT University for providing necessary laboratory facilities for smooth conduct of the work. We also extend our gratitude towards Central Electrochemical Research Institute, Karaikudi, Tamil Nadu, India for the assistance of SEM and EDX analysis.

REFERENCES

1. L. He, B. B. Wang, D. D. Liu, K. S. Qian and H. B. Xu, *Korean J. Chem. Eng.*, **31**, 343 (2014).
2. A. L. Mukherjee, *Environmental Pollution and Health Hazards-causes and control*, Golgotia Publications, New Delhi (1986).
3. S. P. Parker, *Encyclopedia of Environmental Science*, 2nd Ed. McGraw Hill, New York (1980).
4. I. S. Kwak, S. W. Won, S. B. Choi, J. Mao, S. Kim, B. W. Chung and Y. S. Yun, *Korean J. Chem. Eng.*, **28**, 927 (2011).
5. M. Y. Can, Y. Kaya and O. F. Algur, *Bioresour. Technol.*, **97**, 1761 (2006).
6. D. B. Wu, C. J. Niu, D. Q. Li and Y. Bai, *J. Alloy. Compd.*, **374**, 442 (2004).
7. H. Runtti, S. Tuomikoskia, T. Kangas, U. Lassi, T. Kuokkanen and J. Ramo, *J. Water Process Eng.*, **4**, 12 (2014).
8. R. Celis, M. A. Adelano, M. C. Hermosin and J. Cornejo, *J. Hazard. Mater.*, **9**, 67 (2012).
9. A. Hassani, R. D. C. Soltani, S. Karaca and A. Khataee, *J. Ind. Eng. Chem.*, **21**, 1197 (2015).
10. S. M. Dehaghi, B. Rahmanifar, A. M. Moradi and P. A. Azar, *J. Saudi Chem. Soc.*, **18**, 348 (2014).
11. J. H. An and S. Dultz, *Clay Clay Miner.*, **56**, 549 (2008).
12. M. Islam, P. C. Mishra and R. Patel, *J. Hazard. Mater.*, **189**, 755 (2011).
13. H. Jiang, P. Chen, S. Luoa, X. Tua, Q. Cao and M. Shu, *Appl. Surf. Sci.*, **284**, 942 (2013).
14. G. E. Marquez, M. J. P. Ribeiro, J. M. Ventura and J. A. Labrincha, *Ceram. Int.*, **30**, 111 (2004).
15. M. G. A. Vieira, A. F. Almeida Neto, M. L. Gimenes and M. G. C. da Silva, *J. Hazard. Mater.*, **177**, 362 (2010).
16. A. Olgun and N. Atar, *J. Ind. Eng. Chem.*, **18**, 1751 (2012).
17. K. A. Juby, C. Dwivedi, M. Kumar, S. Kota, H. S. Misra and P. N. Bajaj, *Carbohydr. Polym.*, **89**, 906 (2012).
18. D. Das, L. R.Varghese, N. Das, *Desalination*, **360**, 35 (2015).
19. A. S. Kermani and S. Miri, *Korean J. Chem. Eng.* (2015), DOI:10.1007/s11814-014-0285-y.
20. I. Langmuir, *J. Am. Chem. Soc.*, **38**, 2221 (1916).
21. H. M. F. Freundlich, *J. Phys. Chem.*, **57**, 385 (1906).
22. M. M. Dubinin, *Chem. Rev.*, **60**, 235 (1960).
23. Y. S. Ho, *Scientometrics*, **59**, 171 (2004).
24. Y. S. Ho, *Water Res.*, **40**, 119 (2006).
25. D. Das, G. Basak, V. Lakshmi, N. Das, *Biochem. Eng. J.*, **64**, 30 (2012).
26. S. A. Khan, R. Rehman and M. A. Khan, *Waste Manage.*, **15**, 271 (1995).
27. K. Vijayaraghavan and R. Balasubramanian, *Chem. Eng. J.*, **163**, 337 (2010).
28. V. Vinodhini and N. Das, *Desalination*, **264**, 9 (2010).
29. S. Yang, J. Li, D. Shao, J. Hu and X. Wang, *J. Hazard. Mater.*, **166**, 109 (2009).
30. H. Parab, S. Joshi, N. Shenoy, A. Lali, U. S. Sarma and M. Sudersanan, *Process Biochem.*, **41**, 609 (2006).
31. E. Malkoc and Y. Nuhoglu, *J. Hazard. Mater.*, **127**, 120 (2005).
32. E. Malkoc, *J. Hazard. Mater.*, **137**, 899 (2006).
33. S. R. Popuri, Y. Vijaya, V. M. Boddu and K. Abburi, *Bioresour. Technol.*, **100**, 194 (2009).
34. D. Das, N. Das and L. Mathew, *J. Hazard. Mater.*, **184**, 765 (2010).
35. V. T. P. Vinod, R. B. Sashidhar and B. Sreedhar, *J. Hazard. Mater.*, **178**, 851 (2010).
36. C. Jeon and J. H. Cha, *J. Ind. Eng. Chem.* (2014), DOI:10.1016/j.jiec.2014.09.016.
37. D. Charumathi and N. Das, *Desalination*, **285**, 22 (2012).
38. D. Das, J. S. Varshini and N. Das, *Miner. Eng.*, **69**, 40 (2014).